PIO SUSCEPTIBILITY IN FLY-BY-WIRE SYSTEMS

Herlandson Cardoso de Moura*, Gabriel Setim Porto Alegre*, Jorge Henrique Bidinotto*, Eduardo Morgado Belo*
*** University of São Paulo, Engineering School of São Carlos, Brazil. Av. João Dagnone, 1100. 13563-120, phone +55 16 3373-8350**

Keywords: *PIO, Fly-By-Wire, Human pilot models, Model reference, ROVER*

Abstract

The present work proposes to investigate the relationship between the longitudinal dynamics of Fly-by-Wire aircrafts and the resultant susceptibility to the Pilot Induced Oscillations phenomena. Different values of the stability derivatives will be simulated in software implementations with multiple theoretical pilot models. The aircraft movement is considered happen only along the longitudinal axis. It is expected from these trials a range of values of the derivatives that must be avoided in future aircraft designs to minimize the PIO occurrence and which derivatives have influence on PIO occurrence.

1 Introduction

In the last few decades, the automation of aircrafts has been growing fast. Considering it, the developing process must concern about safety and flying qualities of such systems, especially on the called Fly-By-Wire (FBW) which is applied nowadays in large scale. It is extremely helpful in the project development to avoid an undesired response, like Pilot Induced Oscillations (PIO), prior to flight tests of the aircraft. The PIO phenomena can be defined as "sustained or uncontrollable oscillations resulting from the efforts of the pilot to control the airplane" [1]. It has been studied since the 1960s in manual flight control airplanes, as seen in [2-4], that investigate the causes of these events. Another works performed, such as [5,6], studied experimentally human pilot models to predict the proneness to PIO in the simulated systems. Algorithms to detected the occurrence of the phenomena in real time have also been studied, like The Real Time Oscillation Verifier (ROVER), which was defined by [7] and implemented in [8]. Despite these phenomena have been studied for 50 years there are few researches focused on FBW systems. Those issues have motivated the present work, which aims to look for conditions that PIO susceptibility is present for aircrafts with FBW systems, in order to increase the flight safety and quality on aircraft provided with this kind of command.

For FBW systems, the stability derivatives can be implemented via software. Consequently, the resultant response of such aircrafts can be altered prior to flight operation. Considering this scenario, the present work proposes to investigate the relation between the longitudinal dynamic characteristics of FBW airplanes and its susceptibility to PIO. This proneness is investigated with computer simulations, using the Matlab platform and also an integration of this software with commercial flight simulators that can provide a fast visual method to verify the resultant system response. The required dynamics of the simulated aircraft is implemented by the use of a Model Reference Adaptive Control (MRAC), which can alter the original system dynamics to follow the model response.

This paper is organized as follows: the Aircrafts Dynamics Modelling is described in section 2, followed by the controller framework description in Section 3. This chapter also includes a briefly explanation of pilot models in section 3.1 and the ROVER algorithm in Section 3.2. Next, the experimental setup is described in Section 4. Experimental results are then presented in Section 5 and a discussion of these

results is done in Section 6. Finally concluding remarks are discussed in the last section.

2 Aircrafts Modelling: Stability and Control derivatives

An aircraft modelled as a rigid body have six degree of freedom, three of translation (x,y and z) and three of rotational motion angles (roll-ϕ, pitch-θ and yaw-ψ). Commonly, in the flight dynamics formulation an airframe's stability axes O_B located at the aircraft's center of gravity (CG) and moving with it is defined as presented in Fig. (1), which is referenced to a reference frame O_E. Once this airframe is defined, the resultant aerodynamic force can be described by three components [X,Y,Z] acting along each corresponded axis. Similarly, the resultant moment vector has the components [L,M,N] representing the rolling, pitching and yawing moment respectively. The velocity of the aircraft's CG also has the components [u,v,w] and angular velocity the components [p,q,r], which represents the rate of roll, pitch and yaw correspondingly. The linearized equations of aircrafts motion in the longitudinal plane can then be derived considering some simplifying assumptions: the aircraft is treated as a single rigid body with six degrees of freedom; the gyroscopic effects of the spinning rotors are neglected; the wind velocity is considered zero; and finally the longitudinal motion is decoupled of the lateral one. Considering these simplifications and the Etkin[9] formulation, which applies the small-disturbance theory, the linear equations of motion can be defined as a state space model. In the present notation, the variables reference values are represented by a subscript zero and the small perturbations from the reference condition are denoted by the prefix Δ.

The longitudinal aircraft dynamics can be then represented by the equations:

$$\dot{x} = Ax + Bu \qquad (1)$$

$$y = Cx + Du \qquad (2)$$

where the states x is represented by the vector $[\Delta u \quad w \quad q \quad \Delta\theta]^T$ and for a constant throttle control condition the input is defined as the elevator angle position δ_e.

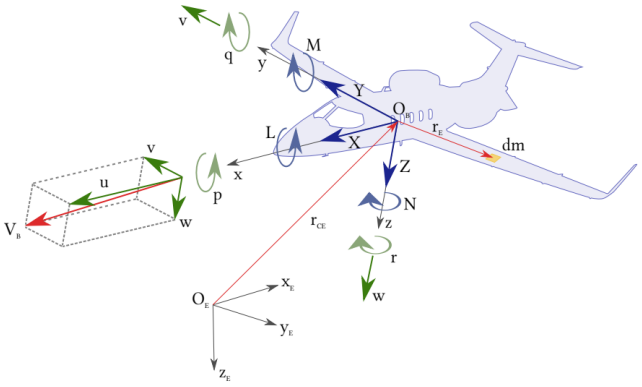

Figure 1: Aircraft Modelling

The expanded expression of Eq. (1) is presented in Eq. (3). The terms $X_u, X_w, Z_u, Z_w, Z_q, Z_{\dot{w}}, M_u, M_q$ and $M_{\dot{w}}$ represent the longitudinal dimensional stability derivatives and the terms $X_{\delta_e}, Z_{\delta_e}$ and M_{δ_e} represent the longitudinal control derivatives. These parameters can also be expressed in a non-dimensional way, which will be expressed in the present work by the variables $C_{x_u}, C_{x_\alpha}, C_{z_u}, C_{z_\alpha}, C_{z_q}, C_{z_{\dot{\alpha}}}, C_{m_u}, C_{m_\alpha}, C_{m_q}, C_{m_{\dot{\alpha}}}$ respectively for the stability derivatives and $C_{x_{\delta_e}}, C_{z_{\delta_e}}$ *and* $C_{m_{\delta_e}}$ for the control derivatives. The stability and control derivatives will be evaluated with different values in the present work, aiming to find the relation between their values and the resultant proneness to the PIO phenomena. The matrixes C and D are defined depending of the output considered. At the present work C is considered an identity matrix and D is a zero matrix, which enables the output to be the states defined, as shown in Eq. (4).

$$\begin{bmatrix}\Delta\dot{u}\\ \dot{w}\\ \dot{q}\\ \Delta\dot{\theta}\end{bmatrix}=\begin{bmatrix}\frac{X_u}{m} & \frac{X_w}{m} & 0 & -g\cos\theta_o\\ \frac{Z_u}{m-Z_{\dot{w}}} & \frac{Z_w}{m-Z_{\dot{w}}} & \frac{Z_q+mu_o}{m-Z_{\dot{w}}} & \frac{-mg\ \sin\theta_o}{m-Z_{\dot{w}}}\\ \frac{1}{I_y}\left[M_u+\frac{M_{\dot{w}}Z_u}{(m-Z_{\dot{w}})}\right] & \frac{1}{I_y}\left[M_w+\frac{M_{\dot{w}}Z_u}{(m-Z_{\dot{w}})}\right] & \frac{1}{I_y}\left[M_q+\frac{M_{\dot{w}}(Z_q+mu_o)}{(m-Z_{\dot{w}})}\right] & -\frac{M_{\dot{w}}mg\ \sin\theta_o}{I_y(m-Z_{\dot{w}})}\\ 0 & 0 & 1 & 0\end{bmatrix}\begin{bmatrix}\Delta u\\ w\\ q\\ \Delta\theta\end{bmatrix}+\begin{bmatrix}\frac{X_{\delta_e}}{m}\\ \frac{Z_{\delta_e}}{m-Z_{\dot{w}}}\\ \frac{M_{\delta_e}}{I_y}+\frac{M_{\dot{w}}}{I_y}\frac{Z_{\delta_e}}{(m-Z_{\dot{w}})}\\ 0\end{bmatrix}\delta_e \quad (3)$$

$$y=\begin{bmatrix}1&0&0&0\\0&1&0&0\\0&0&1&0\\0&0&0&1\end{bmatrix}\begin{bmatrix}\Delta u\\ w\\ q\\ \Delta\theta\end{bmatrix} \quad (4)$$

In order to simulate a more realistic aircraft a simple actuator servo-hydraulic model of the elevator control surface was incorporated to the system. This model enables the modeling of the rate and position saturation of the actuator system and can be described by the diagram showed in Fig. (2). In the normal condition of operation, which occurs when the commands are of small amplitude, the actuator dynamics can be described by Eq. (5).

$$G_{ac}(s)=\frac{1}{\tau s+1} \quad (5)$$

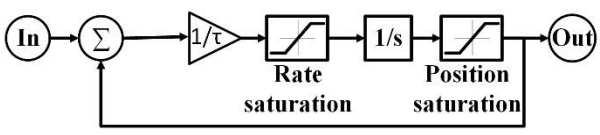

Figure 2: Actuator dynamics

3 Control system framework

The control system structure is showed in Fig. (3). The reference signal, commonly named as synthetic task (Syntask), consists in a sequence of pitch angles to be followed by the simulated aircraft. The error between the reference and actual position of the pitch angle is then sent to a pilot model, which aims to simulate the behavior of a real human pilot. This model so calculates a control signal which is passed to a reference state space model. This model consists of a state space equation, as defined in Eq. (1) and (2), which models the longitudinal dynamics of an aircraft to a given set of values for the stability and control derivatives.

Furthermore, this reference model operates in a closed-loop scheme considering for that the Linear Quadratic Regulator (LQR) methodology. The output of the model is then used to calculate an error signal between its output and the actual output of the controlled aircraft, which in the present work is represented by a flight simulator model. These set of signals is so used in the implementation of the M-MRAC (Modified Model Reference Adaptive Control),

which guarantees that the controlled aircraft follows the model reference dynamics. Lastly, the ROVER algorithm detects the PIO phenomena in real time in the controlled aircraft output. The ROVER output will be then used in the evaluation of the implemented models proneness to the phenomena. The next sections describe each of the cited control system elements.

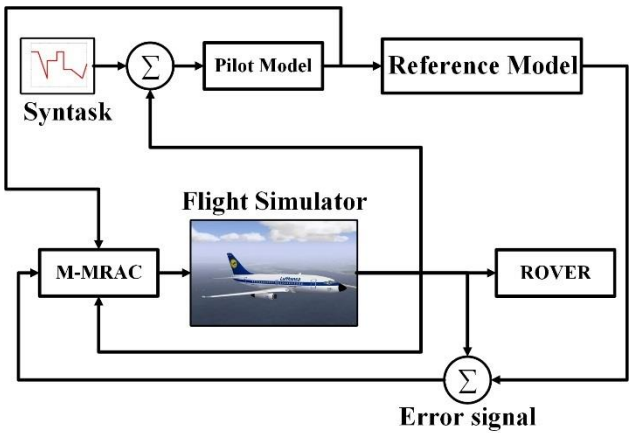

Figure 3: Control system structure

3.1 Pilot Modelling

Due to the ability to adapt its behavior, the field of modelling the human response consists in a challenging and difficult issue. Nevertheless, some transfer functions can simulate the human pilot behavior in simple tasks as the one considered in the present work, where a reference signal of the pitch angle must be tracked. For this purpose, three models will be considered: the Tustin[10] pilot model, the crossover[11] model and the precision[12] pilot model described by the Eqs. (6), (7) and (8) respectively. The input for these models is considered the error $e(s)$ for the tracking task considered and the output is defined as the elevator angle command $\delta_p(s)$.

$$\frac{\delta_p(s)}{e(s)} = \frac{K_p(5s+1)e^{-0.3s}}{s} \qquad (6)$$

$$\frac{\delta_p(s)}{e(s)} = \frac{K_p e^{-0.3s}}{0.2s+1} \qquad (7)$$

$$\frac{\delta_p(s)}{e(s)} = K_p e^{-0.3s}\frac{(6s+1)}{(3s+1)}G_{NM}(s) \qquad (8)$$

$$G_{NM}(s) = \left(\frac{1}{(0.1s+1)\left(\frac{s^2}{20^2}+\frac{2\times 0.7}{20}s+1\right)}\right)$$

3.2 Reference Model: LQR

The reference model presented in Fig. (3) is defined in closed loop scheme using the LQR control strategy. This approach enables the possibility of modification in the original response of the model. Besides, the stability of this system is assured with the LQR control system. For its implementation is aimed, for a given MIMO (Multiple-Input-Multiple-Output) system $\dot{x} = Ax + Bu (x \in \mathbb{R}^n \; and \; u \in \mathbb{R}^m)$, a control law $u = -Kx$ which minimizes the quadratic cost function:

$$J = \int_0^\infty (x^T Q x + u^T R u)dt \qquad (9)$$

where $Q \geq 0$ and $R > 0$ are symmetric, positive semi-definite matrices with appropriated dimensions. The solution for this LQR problem gives the gain K of the form:

$$K = R^{-1}B^T P \qquad (10)$$

to a $P \in \mathbb{R}^{n\times n}$ positive definite, symmetric matrix which satisfies the equation:

$$PA + A^T P - PBR^{-1}B^T P + Q = 0 \qquad (11)$$

However, the LQR problem presented is based on the minimization of a set of signals, commonly known as controlled outputs, in the shortest amount of time. Therefore, some modifications are necessary in order to enable this method to be applied in system which aims to track a reference signal. One of these methods, as stated in [13], adds to the system a new state z of the error between the reference r and the system output, as follows:

$$\dot{z} = r - C_{lqr}x \tag{12}$$

where C_{lqr} denotes a matrix of appropriated dimensions. The system is then altered in a augmented form with the inclusion of the new state:

$$\begin{bmatrix}\dot{x}\\ \dot{z}\end{bmatrix} = \begin{bmatrix}A & 0_{n\times m}\\ -C_{lqr} & 0_{m\times m}\end{bmatrix}\begin{bmatrix}x\\ z\end{bmatrix} + \begin{bmatrix}B\\ 0_{m\times m}\end{bmatrix}u + \begin{bmatrix}0_{n\times m}\\ I_{m\times m}\end{bmatrix}r \tag{13}$$

where *I* represents an identity matrix. Once the augmented system is defined, a control law which minimizes the quadratic cost function presented in Eq. (9) is searched in the form $u = -[K_x \quad K_z]\begin{bmatrix}x\\ z\end{bmatrix}$.

3.3 M-MRAC

The control systems named MRAC (Model Reference Adaptive Control) are a class of algorithms which the desired response of the controlled system is specified by a model. The parameters of the controller are then adjusted based upon the error between the output of the controlled and the model systems. The controller parameters so converge asymptotically to a set of ideal values, which can enable the controlled system to tracks a reference following the dynamics of the model system.

For a MIMO system, $\dot{x} = Ax + Bu (x \in \mathbb{R}^n \; and \; u \in \mathbb{R}^m)$ with $x(0) = x_0$, a MRAC controller can be defined using the inverse Lyapunov analysis, as stated in [14]. The main purpose of the this MRAC system is to design a state feedback adaptive control law so the system state x globally uniformly asymptotically tracks the state $x_{ref} \in \mathbb{R}^n$ of the reference model:

$$\dot{x}_{ref}(t) = A_{ref}x_{ref}(t) + B_{ref}r(t) \qquad x_{ref}(0) = x_0 \tag{14}$$

where $A_{ref} \in \mathbb{R}^{n\times n}$ is a Hurwitz matrix, $B_{ref} \in \mathbb{R}^{n\times m}$ and $r(t) \in \mathbb{R}^m$ is an external bounded command vector. The control input u thus needs to be selected so the tracking error presented in Eq. (15) globally uniformly asymptotically tends to zero.

$$e(t) = x(t) - x_{ref}(t) \tag{15}$$

Through the application of the inverse Lyapunov analysis the control law can be computed as stated in Eq. (16), where $\widehat{K}_x \in R^{n\,X\,m}$ e $\widehat{K}_r \in R^{m\,X\,m}$ are control gains (or adaptive laws) which are generated online with the controller.

$$u = \widehat{K}_x^T x + \widehat{K}_r^T r \tag{16}$$

If the adaptive laws are selected as stated in Eq. (17) a Lyapunov function V can be defined with its time derivative globally negative semidefinite, in the form $\dot{V} = -e^T Qe \leq 0$ (for some $Q = Q^T > 0$), and with its second derivative bounded in the form $\ddot{V} = -2e^T Q\dot{e}$. Consequently, the Lyapunov analysis establishes that the state tracking error $e(t)$ defined in Eq. (15) tends to the origin globally, uniformly and asymptotically. The terms $\Gamma_x = \Gamma_x^T > 0$ and $\Gamma_r = \Gamma_r^T > 0$ are user selected matrices of rate of adaption and $P = P^T > 0$ satisfies the algebraic Lyapunov equation $PA_{ref} + A_{ref}^T P = -Q$ for some $Q = Q^T > 0$.

$$\dot{\widehat{K}}_x = -\Gamma_x x e^T PB \qquad \dot{\widehat{K}}_r = -\Gamma_r r(t) e^T PB \tag{17}$$

Nevertheless, the classical MRAC system described above can have an oscillatory transient behavior which deteriorate the controller response and limits its applicability,

especially in a PIO scenario, where an oscillatory response already exists. To overcome this problem, a simple modification in the reference model can be done by feeding back the tracking error signal. This approach is called modified reference model MRAC or M-MRAC and is defined in [15]. In the M-MRAC framework, the tracking error signal $e_m(t) = x(t) - x_m(t)$ is computed using the modified model reference:

$$\dot{x}_m(t) = A_m x_m(t) + B_m r(t) + \lambda e_m(t) \quad (18)$$
$$x_m(0) = x_0$$

where $\lambda > 0$ is a design parameter. One can notice that for $\lambda = 0$ the conventional MRAC design is achieved again, with $e(t) = e_m(t)$. The application of the Lyapunov stability theory can also prove that the modified state tracking error $e_m(t)$ tends to the origin globally, uniformly and asymptotically. The parameter λ, according to [16] methodology, can be calculated in the terms of the adaption rate matrix Γ_r and the matrix P ($P = P^T > 0$ satisfies the algebraic Lyapunov equation $PA_{ref} + A_{ref}^T P = -Q$ for some $Q = Q^T > 0$) as follows:

$$\lambda = \sqrt{2\alpha\Gamma_r \lambda_{máx}(B_m^T P B_m)} \quad (19)$$

where $\alpha = \|x_0\|^2 + sup_t\|r(t)\|^2$ and $\lambda_{máx}$ is a adjustable parameter.

3.4 ROVER

The ROVER algorithm considered in the present work can detect in real time the occurrence of the PIO phenomena based on the monitoring of four parameters: the amplitude and frequency of the pitch rate aircraft response, the amplitude of the pilot command and the phase angle difference between these signals. If one of these monitored parameters exceed the values presented in Table (1) the value 1 is set to a corresponded flag. When the four flags are set with 1 a severe PIO condition occurs. The implemented ROVER algorithm gives then a signal which in the PIO condition (four flags set) has the value one, otherwise it has a zero value.

Table 1. ROVER parameters

Parameter	Threshold value
Pitch rate magnitude	$\geq 12^o$ /s
Pitch rate frequency	1 – 10 rad/s
Pilot command	$\geq$ 1.2 peak-to-peak (60% of maximum deflection)
Phase difference	$\geq 180^o$

4 Methodology

In order to investigate the relation between the longitudinal stability /control derivatives and the resultant proneness of the implemented aircraft dynamics to the PIO, simulations of the described system are performed in the software Matlab. The aircrafts models implemented in the simulations are based on the flight data of the model Boeing 747-100, derived from [9], in a cruising and horizontal flight condition at a fixed altitude of 40000 ft at a Mach Number of 0,8. The original stability and control derivatives of this aircraft model is shown in Table (2).

Table 2. Boeing 747-100 Stability/ Control Derivatives

Derivative	Value	Derivative	Value
C_{x_u}	-0.108	C_{m_α}	-1.023
C_{x_α}	0.219	C_{m_q}	-23.921
C_{z_u}	-1.414	$C_{m_{\dot{\alpha}}}$	-6.315
C_{z_α}	-4.920	$C_{x_{\delta_e}}$	-3.818 x 10^{-6}
C_{z_q}	-5.923	$C_{z_{\delta_e}}$	-0.365
$C_{z_{\dot{\alpha}}}$	5.896	$C_{m_{\delta_e}}$	-1.444
C_{m_u}	0.104		

In the first stage of the present work, the longitudinal stability /control derivatives derived from this flight condition data are then variated individually to different values and a state space reference model dynamic is then derived from these altered values. Simulations are performed

considering just the reference model operating in a closed loop condition with the LQR system architecture described in Section 3 for different pilot models. The reference models implemented in this stage also include the actuator dynamics described in Section 2. The proneness of each reference model obtained to the PIO is then evaluated based on the output of the ROVER algorithm, which is expressed as a percentage level of activation of the algorithm in the time interval considered. It is expected of these simulations a range of values for each derivative which must be avoided in order not to occur the phenomena.

In the second stage of the work, sets of combination of these derivatives obtained from the last stage are derived, with low and high proneness to the PIO. Reference models are so calculated from these values, and the complete control architecture with the M-MRAC system described in Section 3 is simulated. The Boeing 777-200 model implemented in the flight simulator software *FlightGear* is considered as the controlled system in this stage. The resultant proneness to the PIO of the controlled aircraft is then evaluated based on the ROVER activation again. These simulations aim to confirm the influence of some of the derivatives in the resulting response of the controlled system. Furthermore, the flight simulator can also provide a fast visual method to verify the occurrence of oscillations in the resultant system response.

5 Results

In the first step, simulations are performed using the state space models in order to obtain a range of derivatives, with high proneness to PIO, to be avoided for each pilot model considered. These ranges obtained, for the stability and control derivatives, as result of this process are shown in Tables (3) ,(4) and (5) for Tustin, Crossover and Precision pilot models respectively. In these tables the ROVER range obtained, with its minimum and maximum values, for each corresponded derivative is also presented. The values expressed in parentheses stablishes the corresponded derivative value for the PIO level stablished.

Table 3. Range with high proneness to Tustin Pilot Model

Stability / Control Derivative	Non-dimensional range	ROVER Range Level (%)
C_{m_q}	-20.24 28.30	8.40 (-7.25) 12.82 (-4.07)
$C_{m_{\dot{\alpha}}}$	-3.55 46.13	6.19 (-3.30) 6.34 (45.94)
$C_{z_{\delta_e}}$	-99.11 -93.03	10.64 (-95.51) 10.89 (-94.07)
$C_{m_{\delta_e}}$	1.32 1.41	10.47 (1.37) 12.72 (1.36)

Table 4. Range with high proneness to Crossover Pilot Model

Stability / Control Derivative	Non-dimensional range	ROVER Range Level (%)
C_{m_q}	-12.49 28.30	14.73 (28.30) 14.81 (-7.25)
$C_{m_{\dot{\alpha}}}$	6.01 25.21	14.73 (23.09) 14.82 (9.76)
$C_{z_{\delta_e}}$	-116.19 -96.44	20.70 (-96.44) 51.30 (-97.56)
$C_{m_{\delta_e}}$	1.22 1.48	14.81 (1.47) 14.87 (1.39)

Table 5. Range with high proneness to Precision Pilot Model

Stability / Control Derivative	Non-dimensional range	ROVER Range Level (%)
C_{m_q}	-23.25 28.30	10.32 (27.20) 14.70 (-21.10)
$C_{m_{\dot{\alpha}}}$	-5.55 45.05	10.31 (44.06) 10.42 (-4.12)
$C_{z_{\delta_e}}$	-146.79 -89.08	10.78 (-146.54) 61.56 (-93.68)
$C_{m_{\delta_e}}$	1.07 1.54	10.36 (1.53) 15.63 (1.22)

Considering the values obtained for each stability/control derivative, general ranges could be derived for an independent pilot model system. These ranges are presented in Table (6).

Furthermore, the proposed method can enable one to find also a range of values with low proneness to the phenomena. These values are presented in Table (7).

Table 6. General range with high proneness

Stability / Control Derivative	Non-dimensional range
C_{m_q}	-12.49 28.30
$C_{m_{\dot{\alpha}}}$	6.01 25.21
$C_{z_{\delta_e}}$	-99.11 -96.44
$C_{m_{\delta_e}}$	1.22 1.41

Table 7. General range with low proneness

Stability / Control Derivative	Non-dimensional range
C_{z_q}	463.74 1.15 x 10^3
$C_{z_{\dot{\alpha}}}$	328.97 819.48
C_{m_α}	-2.29 -1.74
C_{m_q}	-141.61 -65.07
$C_{m_{\dot{\alpha}}}$	-89.73 -51.65
$C_{z_{\delta_e}}$	51.07 2.12 x 10^3
	-1.98 x 10^3 -299.14
$C_{m_{\delta_e}}$	1.88 93.28
	-97.90 -2.02

In the second step simulations were performed with the M-MRAC system integrated with the flight simulator *FlightGear* described in section (3). The reference models were built applying the ranges founded with low and high proneness. The original model was also simulated in order to compare the PIO level obtained. The high proneness model was set with $\boldsymbol{C_{m_q} = -6.92}$, $\boldsymbol{C_{m_{\dot{\alpha}}} = 11.91}$, $\boldsymbol{C_{z_{\delta_e}} = -97.12}$ and $\boldsymbol{C_{m_{\delta_e}} = 1.32}$. The low proneness model was set with $\boldsymbol{C_{z_q} = 740.33}$, $\boldsymbol{C_{z_{\dot{\alpha}}} = 616.68}$and $\boldsymbol{C_{m_{\delta_e}} = 1.88}$. The others stability/control derivatives of these models were maintained with its original values. The Figs. (4), (5) and (6) present the plot response of the simulations performed. In these figures the PIO level obtained to each model considered is also shown, which was multiplied by a factor of ten to facilitate the visualization.

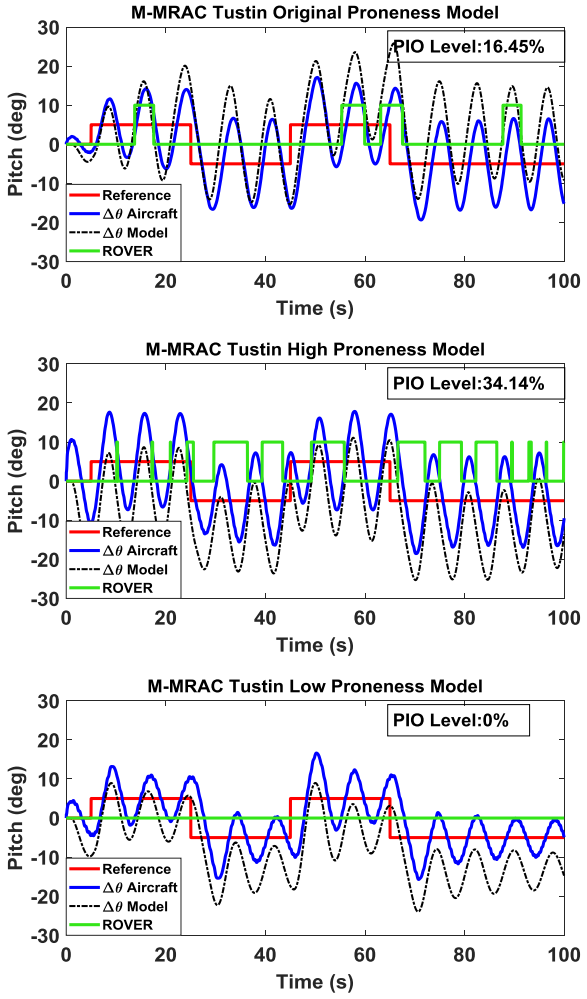

Figure 4: M-MRAC+ Flight Simulator: Tustin Pilot Model

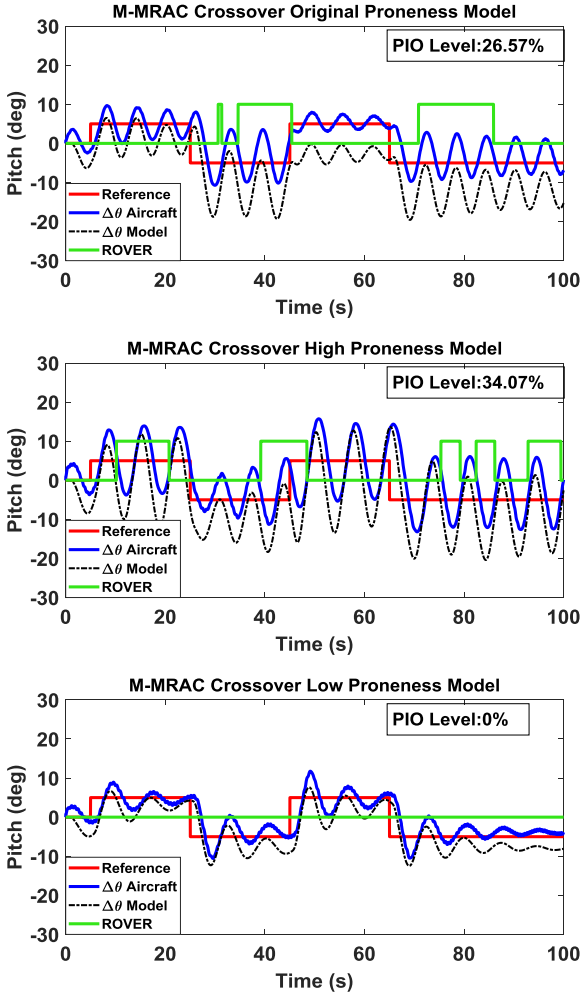

Figure 5: M-MRAC+ Flight Simulator: Crossover Pilot Model

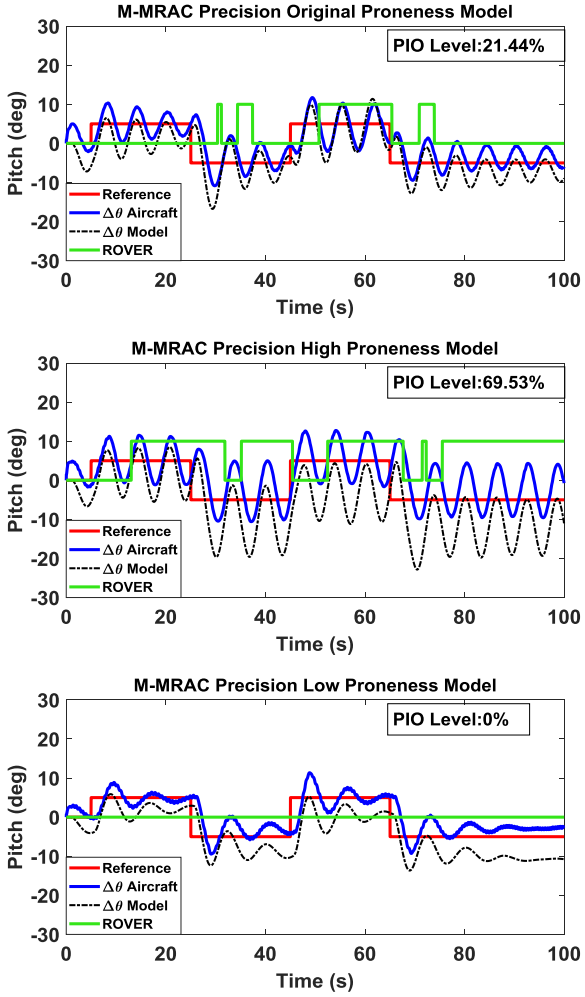

Figure 6: M-MRAC+ Flight Simulator: Precision Pilot Model

6 Discussions

In the first step of the present work simulations were performed with the purpose of obtaining ranges for the stability/control derivatives with high proneness to PIO. In this stage, the original derivatives values (presented in Table (2)) were varied and the resultant proneness of the system was evaluated. For this intent, a closed loop system was simulated consisting in the state space model of the aircraft, a LQR controller and the ROVER algorithm. The system also included a pilot model described function in order to simulate a more realistic scenario. In this stage, to obtain the high proneness derivatives, the system was first simulated with its original derivatives values with the pilot gain adjusted on the onset of a PIO condition, based on the ROVER signal.

The PIO level obtained in this condition is then used as a reference to be compared with the values obtained with the variation of the derivatives. The resultant state space model, obtained from the derivatives variation, is then considered as a high proneness if leads to a response with a greater ROVER level activation. For the Tustin pilot model, a gain of $K_p = 1.185$ led the original state space system to a PIO level of activation of 0% (percentage of the time duration of the simulation). As presented in Table (3) the most sensitive derivatives are C_{m_q}, $C_{m_{\dot{\alpha}}}$, $C_{z_{\delta_e}}$ and $C_{m_{\delta_e}}$. This result was partially expected, since these derivatives appears directly in the expressions of q and $\Delta\theta_0$ in the state space modelling presented in Section (2). The variation of the other derivatives led the model to unsatisfactory responses, and then are not

considered in the present work. In this case, for instance, the adjustment of the derivative C_{m_q} to a value of $C_{m_q} = -4.07$ leads the system to a PIO condition with a ROVER level of 12.82 %. For the Crossover Pilot model a gain of $K_p = 6.185$ make the original system to operate in a PIO level condition of 2%. The most propense derivative, in this case, was $C_{z_{\delta_e}} = -97.56$ which results in a system with a ROVER level of 51.30 %. In the last pilot describe function considered, the Precision model, a gain of $K_p = 4$ make the original system to operate in a PIO level condition of 1.93%. The most propense derivative was then $C_{z_{\delta_e}} = -93.68$, which leads to a system with a ROVER level of 61.56 %.

Once these ranges, with high proneness, were obtained, the analysis of the Tables (3), (4) and (5) can lead one to determinate a general range, for each derivative considered, with high proneness to the phenomena, which is independent of the pilot model considered. These range values are shown in Table (6). The relevance of the method developed in the present work resides in the fact that it is independent of the control system architecture considered. Therefore, it can be applied to any control system considered, just by varying the derivatives values and evaluating the resultant proneness to PIO. Besides, the method can enable one also to find ranges for the derivatives with low proneness to the phenomena. For this case, the pilot gain of the models is adjusted with higher values in order to obtain a severe PIO condition. The derivatives are then variated, and their corresponded values are considered to be part of a low proneness model if lead the system to a lower ROVER activation level. The ranges obtained for this case are present in Table (7). As can be noticed by comparing the Tables (6) and (7), the same derivatives of the high proneness case can lead the system to a low proneness condition. The difference resides just in the ranges considered.

In the second stage of the work, simulations with commercial flight simulator software were performed in order to confirm the effectiveness of the proposed method. In this step, the M-MRAC control system architecture described in Section (3) was applied. The values obtained in Table (6) for the derivatives were combined, and a high proneness model was stablished. In a similar procedure, a low proneness model was obtained from the results of Table (7). The original state space system and these new systems obtained are then used as reference models to the M-MRAC system. Each resultant system was then simulated with the same pilot models considered in the first step with high gains to incite a severe PIO condition. The controlled plant, in this case, is considered the aircraft dynamics model of the flight simulator. In fact, as can be noticed from the results illustrated in Figs. (4), (5) and (6), the high proneness model led the system to a more severe PIO condition for the three pilot models considered, since the ROVER level was greater for this case. On the other hand, the low proneness model built made the system to stop the PIO occurrence, which confirm the efficacy of the method.

7 Conclusions

The method proposed in the present work can enable one to find the ranges for the stability/control derivatives more propense to the PIO phenomena. The method can be employed to any control system architecture applied to create a closed loop system with the state space model considered, since it is based on the outputs of the resultant system. The proposed system can also be applied to determine low proneness models and to any pilot model considered. Furthermore, its effectiveness can be confirmed with the proposed M-MRAC system integrated with commercial flight simulators, which can improve the analysis of the resultant system by the use of the visualization of the aircraft response in real time. Besides, considering the system is already integrated with a flight-simulator, future works can be performed with human pilots using the visual feedback provided by a full flight simulator, including the architectures integrated with movable platforms.

References

[1] DEPARTMENT OF DEFENSE INTERFACE STANDARD. Mil Standard, MIL1797A: *Flying Qualities of Piloted Airplanes*. Washington D. C., 1995.

[2] ASHKENAS, I. L.; JEX, H. R.; MCRUER, D. T. *Pilot-induced oscillations: their cause and analysis*. SYSTEMS TECHNOLOGY INC INGLEWOODCA, 1964.

[3] SMITH, J. W.; BERRY, D. T. *Analysis of longitudinal pilot-induced oscillation tendencies of YF-12 aircraft*. 1975.

[4] ANDERSON, M. R. Pilot-Induced Oscillations Involving Multiple Non-linearities. *Journal of Guidance Control and Dynamics*, v. 21, n. 5, p. 786-791, 1998.

[5] TOADER, A.; URSU, I. Pilot Modeling Based on Time-Delay Synthesis. *Proceedings of the Institution of Mechanical Engineering Part G - Journal of Aerospace Engineering*, v. 228, n. 5, p. 740-754, 2014.

[6] ACOSTA, D. M.; YILDIRAY, Y.; CRAUN, R. W.; BEARD, S. D.; LEONARD, M. W.; HARDY, G. H.; WEINSTEIN, M. Pilot Evaluation of a Control Allocation Technique to Recover from Pilot-Induced Oscillations. *Journal of Aircraft*, v. 52, n. 1, p. 130-140, 2015.

[7] MITCHELL, D. G.; ARENCIBIA, A. J.; MUNOZ, S. Real-time detection of pilot-induced oscillations. In: *AIAA Atmospheric Flight Mechanics Conference and Exhibit*, Providence, Rhode Island, p. 4700, 2004.

[8] JOHNSON, D. A. *Suppression of pilot-induced oscillation (PIO)*. AIR FORCE INST OF TECH WRIGHT-PATTERSON AFB OH SCHOOL OF ENGINEERING AND MANAGEMENT, 2002.

[9] ETKIN, B.; REID, L. D. *Dynamics of flight stability and control*. 3rd Edition. New York: New York Wiley, 1996.

[10] TUSTIN, A. The nature of the operator's response in manual control, and its implications for controller design. *Journal of the Institution of Electrical Engineers-Part IIA: Automatic Regulators and Servo Mechanisms*, v. 94, n. 2, p. 190-206, 1947.

[11] MCRUER, D. T.; KRENDEL, E. S. Mathematical models of human pilot behavior. *Advisory Group For Aerospace Research And Development*. Neuilly-Sur-Seine (France), 1974.

[12] MCRUER, D. T., Graham, D., Krendel, E., and Reisener, W., *Human Pilot Dynamics in Compensatory Systems. Air Force Flight Dynamics*. Lab. AFFDL-65-15. 1965.

[13] GHAFFAR, Alia Abdul; RICHARDSON, Tom. Model reference adaptive control and LQR control for quadrotor with parametric uncertainties. *World Academy of Science, Engineering and Technology, International Journal of Mechanical, Aerospace, Industrial, Mechatronic and Manufacturing Engineering*, v. 9, n. 2, p. 244-250, 2015.

[14] EUGENE, Lavretsky; KEVIN, Wise. *Robust and adaptive control with aerospace applications*. 1st Edition. London, Springer, 2013.

[15] STEPANYAN, Vahram; KRISHNAKUMAR, Kalmanje. MRAC revisited: guaranteed performance with reference model modification. In: *American Control Conference (ACC), 2010. IEEE*, 2010. p. 93-98.

[16] STEPANYAN, Vahram; KRISHNAKUMAR, Kalmanje. On the Robustness Properties of M-MRAC. In: Infotech@ Aerospace. 2012.

Acknowledgments

This work is supported by São Paulo Research Foundation (FAPESP), Grant 2016/16808-5, and by the National Council for Scientific and Technological Development (CNPq).

Contact Author Email Address

Herlandson C. de Moura: herlandsonc@usp.br
Gabriel S. Porto Alegre: gabriel.alegre@usp.br
Jorge H. Bidinotto: jhbidi@sc.usp.br
Eduardo M. Belo: belo@sc.usp.br

Copyright Statement